Attribution of the Extreme U.S. East Coast Snowstorm Activity of 2010

YEHUI CHANG,* SIEGFRIED SCHUBERT, AND MAX SUAREZ

Global Modeling and Assimilation Office, NASA Goddard Space Flight Center, Greenbelt, Maryland

(Manuscript received 22 June 2011, in final form 14 October 2011)

ABSTRACT

This study examines the cause of the extreme snowstorm activity along the U.S. East Coast during the winter of 2009/10 with a focus on the role of sea surface temperature (SST) anomalies. The study employs the Goddard Earth Observing System, version 5 (GEOS-5) atmospheric general circulation model (AGCM) run at high resolution and forced with specified observed or idealized SST. Comparisons are made with the winter of 1999/2000, a period that is characterized by SST anomalies that are largely of opposite sign.

When forced with observed SSTs, the AGCM response consists of a band of enhanced storminess extending from the central subtropical North Pacific, across the southern United States, across the North Atlantic, and across southern Eurasia, with reduced storminess to the north of these regions. Positive precipitation and cold temperature anomalies occur over the eastern United States, reflecting a propensity for enhanced snowstorm activity. Additional idealized SST experiments show that the anomalies over the United States are, to a large extent, driven by the ENSO-related Pacific SST. The North Atlantic SSTs contribute to the cooler temperatures along the East Coast of the United States, while the Indian Ocean SSTs act primarily to warm the central part of the country.

It is further shown that the observed upper-tropospheric height anomalies have a large noise (unforced) component over the Northern Hemisphere, represented over the North Atlantic by a North Atlantic Oscillation (NAO)-like structure. The signal-to-noise ratios of the temperature and precipitation fields nevertheless indicate a potential for predicting the unusual storm activity along the U.S. East Coast several months in advance.

1. Introduction

Major snowstorms affecting the East Coast of the United States (often referred to ''nor'easters'') occur infrequently, though when they do occur, they have major societal impacts, including major disruptions to travel and, at times, loss of life. Famous examples (NWS 2011) include the Washington–Jefferson storm of 1772, the Great Blizzard of 1888 (also known as the White Hurricane), the Knickerbocker storm of 1922 (with more than 100 people killed in the collapse of the Knickerbocker Theater in Washington, D.C.), and the 1993 ''storm of the century'' (with 200 deaths and an estimated two billion U.S. dollars in damages and snow removal costs).

The winter of 2009/10 adds to the list of years with major snowstorms not as a single event, but as a series of storms that together produced one of the snowiest winters in recorded history along the East Coast. Three major snowstorms hit the East Coast during that winter. The first occurred on 18–19 December 2009, blanketing the East Coast with snow, including more than 16 in. of snow in the Washington, D.C. area. The second storm occurred along the East Coast during 5–6 February 2010 [with snow totals at the major airports listed as Baltimore–Washington International Thurgood Marshall Airport (BWI) 25.0 in., Ronald Reagan Washington National Airport (DCA) 17.8 in., Washington Dulles International Airport (IAD) 32.4]. The third storm occurred during 9–10 February, again dumping more than a foot of snow over much of the East Coast. About 50 in. of snow fell in Baltimore during February, making it the single snowiest month in the history of Baltimore since snowfall records began in 1893 (NWS 2011).

A number of studies have addressed the causes of such extreme weather events, in particular, whether there are large-scale circulation anomalies that favor

* Additional affiliation: Goddard Earth Sciences Technology and Research, Morgan State University, Baltimore, Maryland.

Corresponding author address: Siegfried Schubert, Global Modeling and Assimilation Office, NASA Goddard Space Flight Center, NASA/GSFC Code 610.1, Greenbelt, MD 20771.
E-mail: siegfried.d.schubert@nasa.gov

DOI: 10.1175/JCLI-D-11-00353.1

the development of East Coast snowstorms. Serreze et al. (1998) showed that positive extremes of the Pacific–North America (PNA) pattern are associated with enhanced snowfall over the Southeast, Midwest, and mid-Atlantic states when the eastern United States is dominated by a strong 500-hPa trough and lower temperatures. Smith and O'Brien (2001) showed that in the northeastern United States, less (more) snowfall occurs during the cold (warm) phase of ENSO. Schubert et al. (2008) quantified the impact of ENSO on the intensity of winter extreme precipitation events over the contiguous United States. Based on an extreme value analysis of daily winter precipitation, they showed that intense East Coast storms that occur on average only once every 20 yr (20-yr storms) would occur on average in half that time under sustained El Niño conditions, while under La Niña conditions, 20-yr storms would occur on average about once in 30 yr.

The 2009/10 winter was characterized by an El Niño and a persistent negative North Atlantic Oscillation (NAO)–Arctic Oscillation (AO). Seager et al. (2010) used a regression analysis to quantify the relationships between ENSO and NAO events, and seasonal snowfall anomalies in the United States. Based on those results, they concluded that during 2009/10, the high levels of snow in the mid-Atlantic states as well as those in northwest Europe were forced primarily by the negative NAO (and the associated colder temperatures) and to a lesser extent by the El Niño. Similar conclusions were reached by Hoerling (2010), with that study also emphasizing the key role of the NAO in eastern U.S. snowfall through its impact on surface temperature in the metropolitan East Coast. In the NAO blocked (negative) phase, the snow–rain line shifts eastward, so that the eastern United States becomes colder than normal, resulting in snow rather than rain. They note that El Niño also produces a cooling effect on the eastern seaboard (though this effect is weaker than that produced by the NAO).

In this study we revisit the cause of the enhanced snowstorm activity during 2009/10 using high-resolution atmospheric general circulation model (AGCM) simulations forced by observed and idealized sea surface temperature anomalies, with the aim of quantifying the impacts of the Pacific, Atlantic, and Indian Ocean SST anomalies. Section 2 describes the AGCM and simulations. The results are presented in section 3. The summary and conclusions are given in section 4.

2. The GEOS-5 AGCM experiments and validation data

The Goddard Earth Observing System, version 5 (GEOS-5) AGCM (Rienecker et al. 2008) employs the finite-volume dynamics of Lin (2004). This dynamical core is integrated with various physics packages (Bacmeister et al. 2006) under the Earth System Modeling Framework (Collins et al. 2005), including the Catchment Land Surface Model (Koster et al. 2000), and a modified form of the relaxed Arakawa–Schubert convection scheme described by Moorthi and Suarez (1992). For the experiments described here, the model is run with 72 hybrid-sigma vertical levels extending to 0.01 hPa and with either ½° or ¼° horizontal resolution on a cubed sphere.

While our focus is on the winter of 2009/10 (December–February), our analysis consists of a comparison between that winter and another winter (1999/2000), characterized by SST anomalies that are largely of opposite sign (see Fig. 1). In fact, the difference fields (2009/10 − 1999/2000 divided by two) do indeed look very similar to the 2009/10 winter SSTs. We do this for practical reasons—we do not have a long climate simulation with the GEOS-5 AGCM at these resolutions, which we would otherwise use to compare with the 2009/10 results.

The various experiments are listed in Table 1. Information is provided on the model resolution, initial dates for the hindcasts, and the specified SST. In each case, 50 ensemble members were produced. These differed from each other by adding perturbations to the base initial atmospheric conditions [taken from the National Aeronautics and Space Administration's (NASA's) Modern-Era Retrospective Analysis for Research and Applications (MERRA; Rienecker et al. 2011)]. The perturbations are computed from a previously completed November simulation and consist of the scaled (divided by 8) differences between two (randomly chosen) model atmospheric states that are 1 day apart. The initial land state (also from MERRA) does not vary among the ensemble members.

Our initial set of runs (A′ and B′) were done at ¼° horizontal resolution to ensure that the winter storms would be adequately resolved. The remaining simulations were done at ½° since (as we shall show) the basic results were not strongly impacted by the reduction in resolution, and this allowed running a larger set of additional simulations.

In addition to comparing the model results to MERRA, we compare with other observations consisting of the monthly mean (2.5° latitude × 2.5° longitude) Global Precipitation Climatology Project (GPCP version 2) precipitation data documented in Adler et al. (2003), and a gridded high-resolution (0.5° latitude × 0.5° longitude) National Oceanic and Atmospheric Administration surface temperature dataset documented in Fan and Van den Dool (2008).

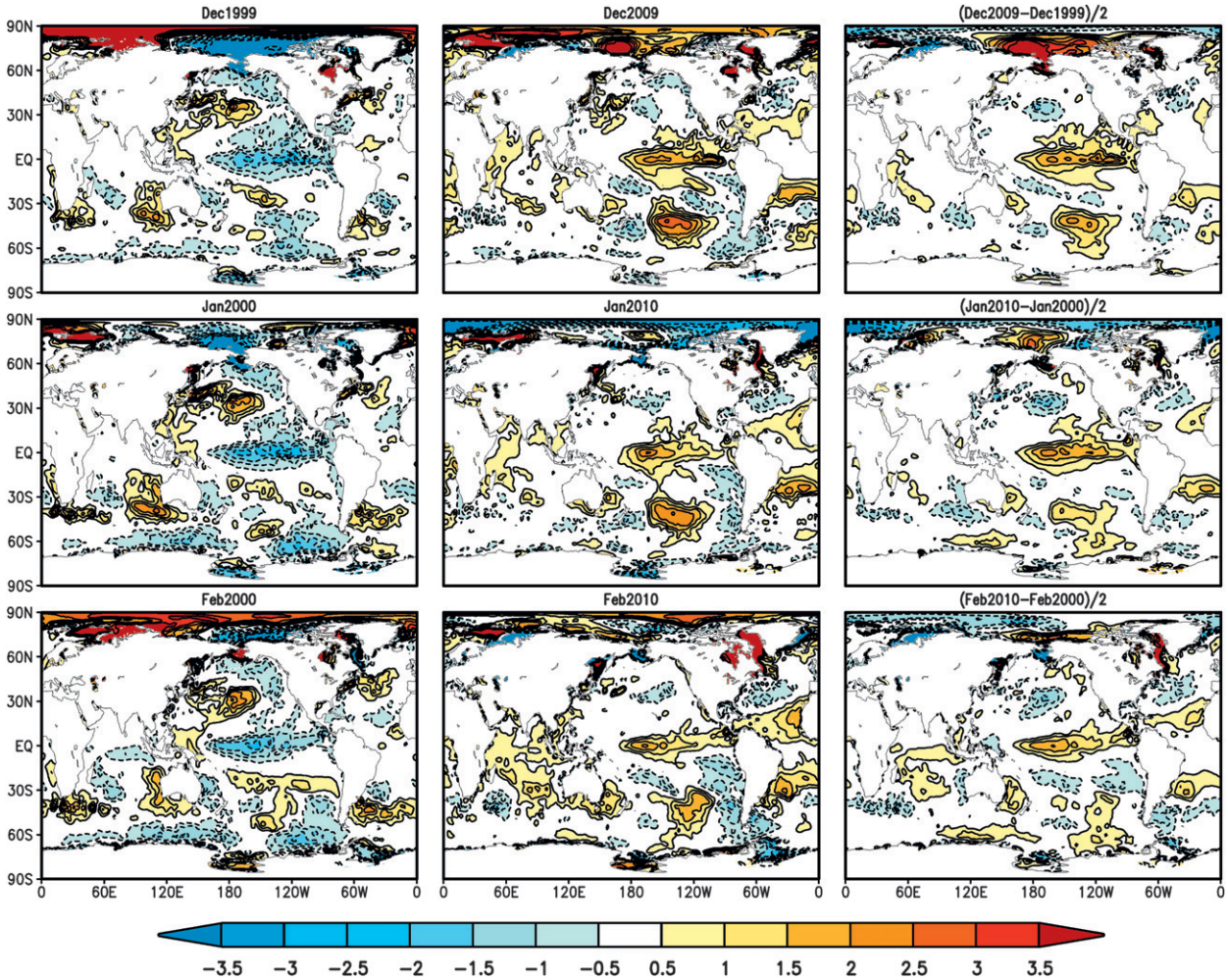

FIG. 1. SST anomalies with respect to the long-term mean (December 1979–February 2010): (left) December–February of 1999/2000, (middle) December–February of 2009/10, and (right) the difference fields (2009/10 − 1999/2000) divided by 2. Units: °C.

3. Results of the GEOS-5 hindcasts

a. Impact of observed SST

Figure 1 shows that during 2009/10, positive SST anomalies existed in the tropical Pacific throughout the winter as part of an evolving El Niño, with anomalies exceeding 2°C throughout the eastern equatorial Pacific in December. During January and February, the structure of the SST anomalies evolved so that the largest positive anomalies were confined to the central equatorial Pacific. The North Atlantic SST anomalies resemble a tripole structure that is also associated with the negative phase of the NAO, with positive SST anomalies in the high latitudes, negative anomalies in the mid-latitudes, and positive anomalies in the subtropics. Other noteworthy SST anomalies are the persistent positive anomalies in the Indian Ocean, the positive anomaly in the South Pacific, and another positive anomaly in the South Atlantic. During the 1999/2000 boreal winter, the SST anomalies are to a large extent of opposite sign. The Pacific is dominated by a La Niña in the tropics, with negative anomalies in the eastern Pacific

TABLE 1. The GEOS-5 AGCM hindcast experiments. The "switched NA" runs have the SST fields in the Atlantic (between 10°S and 75°N) switched between the two winters. The "switched Ind" runs have the SST fields in the Indian Ocean switched between the two winters. Each run has 50 ensemble members. The primes indicate a model horizontal latitude–longitude resolution of 1/4°. All other runs were done at 1/2°.

Resolution (°lat × °lon)	Initial date		SST
	1 Dec 1999	1 Dec 2009	
0.25 × 0.25	A′	B′	Observed
0.50 × 0.50	A	B	Observed
0.50 × 0.50	C	D	Switched NA
0.50 × 0.50	E	F	Switched Ind

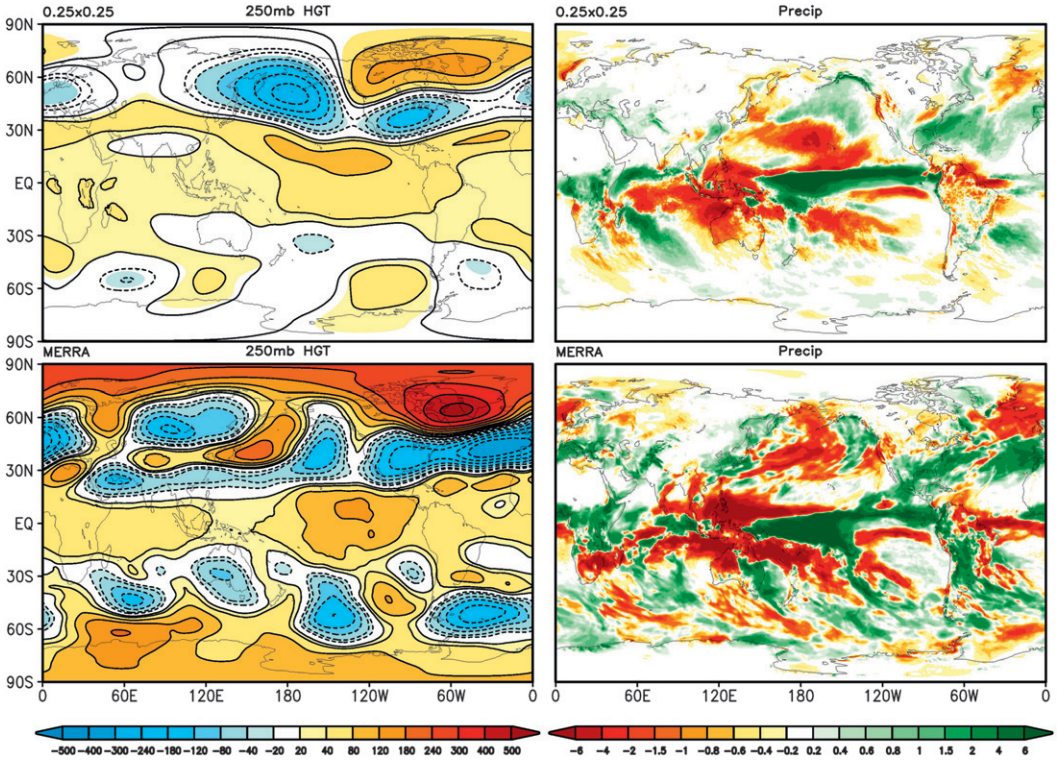

FIG. 2. (top) Fifty-member ensemble mean of GEOS-5 hindcasts run at 0.25 × 0.25 resolution. The results are the differences between February 2010 and February 2000. (left) Height differences at 250 mb (m), and (right) precipitation differences (mm day^{-1}). (bottom) As in (top), but from the MERRA reanalysis.

extending north into the Gulf of Alaska (with positive anomalies to the west) resembling the Pacific decadal oscillation (PDO). The Atlantic SST anomalies are less well defined, though they also show a tendency to be of opposite sign to those that occurred during the 2009/10 winter. The difference fields highlight their similarity to the 2009/10 winter SST anomalies.

We begin by showing the ensemble-mean results from the ¼° experiments. We focus on the February results—this is two months into the runs, which all started on 1 December, so any signal in the ensemble mean should be a response to the SST forcing, since memory of the atmospheric initial conditions is unlikely to play a role at such long lead times.

Figure 2 shows the 250-hPa height and precipitation anomalies computed as the difference between the two Februaries (2010 − 2000). The ensemble-mean model results are compared with what actually occurred as estimated from MERRA. The height response is characterized by what is to a large extent a well-known response to El Niño (e.g., Hoerling and Kumar 2002), with an anomalous trough over the North Pacific, a positive height anomaly over Canada, and a negative anomaly over the United States. An unusual aspect of the response is the extension of the anomalies eastward across the Atlantic and into Europe, a region not typically associated with a strong ENSO signal. The MERRA reanalysis shows generally similar features though noisier and with larger amplitude. In particular, there is a short-wave (wavenumbers 5 and 6) anomaly that extends from Asia across the Pacific that is absent from the ensemble mean. Also, the Southern Hemisphere shows considerably more wave structure than the model results. Nevertheless, the basic structure of the height anomalies that occur over North America, the Atlantic, and Europe is quite consistent with the model's ensemble-mean anomaly patterns.

The ensemble-mean model and MERRA precipitation anomalies (Fig. 2) also show very consistent features. Both show a clear ENSO response in the Pacific, with enhanced precipitation in the central tropical Pacific and reduced precipitation to the north and south and to the west over the region of the warm pool. Focusing on the Northern Hemisphere, both also show enhance precipitation in the southeastern United States and extending northward along the East Coast, suggesting enhanced storm activity in this region. The positive precipitation anomalies extend eastward from the United States, across the Atlantic, and into southern Europe and Asia. Other regions of reduced precipitation include the

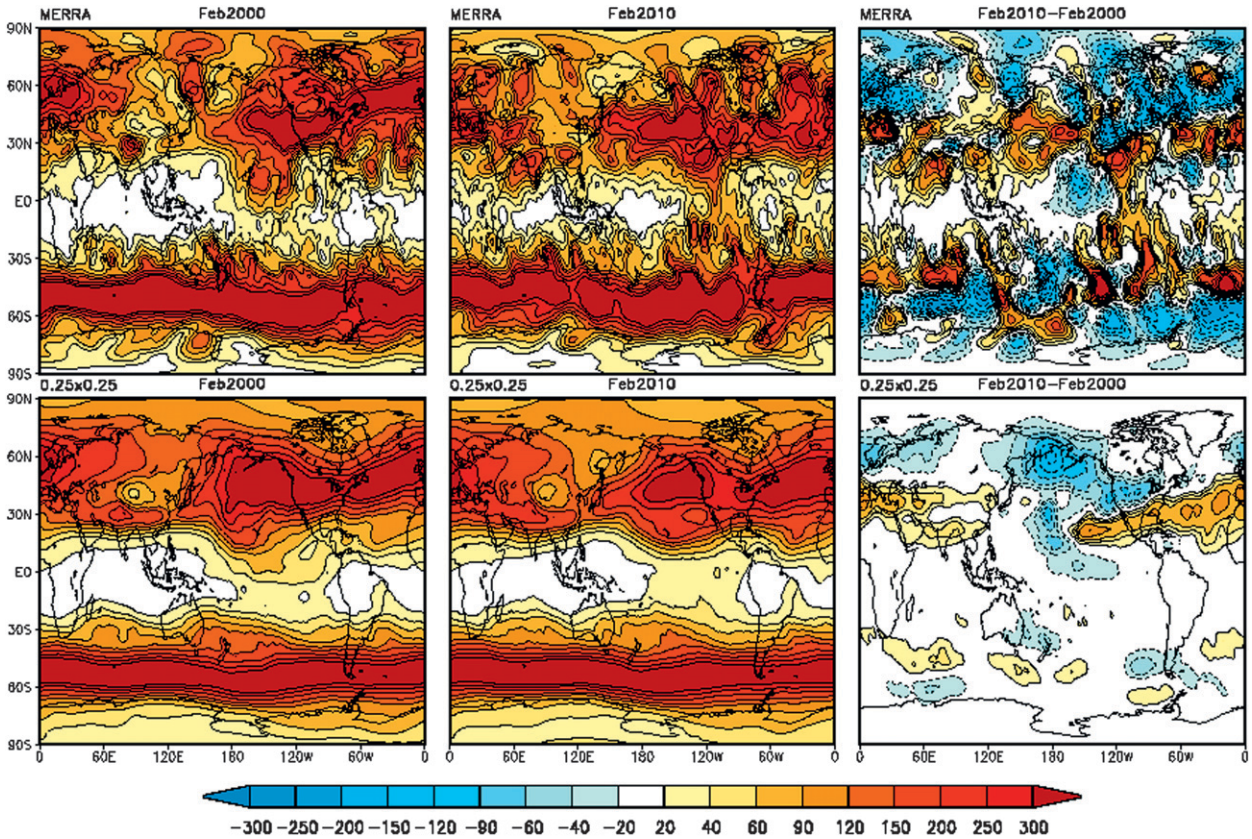

FIG. 3. Monthly-mean daily meridional wind variance $\overline{v'^2}$ at 250 mb: (top) MERRA and (bottom) model simulations (50 ensemble members run at 1/4°) for (left) Feb 2000, (middle) Feb 2010, and (right) Feb 2010 − Feb 2000.

West Coast and the Great Lakes region of the United States, the east coast of Greenland, the North Atlantic–Greenland Sea, and Norway.

Figure 3 quantifies the change in storminess in terms of the February submonthly 250-mb v wind variance computed from daily data. The model results show a band of enhanced storminess extending from the central subtropical North Pacific, across the southern United States into southern Europe, and across southern Asia. Areas of reduced storminess occur in the high latitudes of the North Pacific, across the United States and Canada, and northern Europe and Russia. The observations (the MERRA reanalysis) are generally consistent with the model results, though again they are noisier and are missing the large negative anomaly in the North Pacific—consistent with the differences in the height field anomalies (see Fig. 2).

While model deficiencies may explain some of the discrepancies with the reanalysis, it is likely that many of the differences reflect the fact that the model results are an ensemble mean, while the reanalysis is an estimate of a single realization of nature that contains both a forced part and an unforced (or noise) part. We will address these issues in section 3c in the context of predictability.

We next focus more closely on the impacts over the continental United States and compare the results from the 1/4° and 1/2° runs. Figure 4 shows the simulated ensemble-mean precipitation[1] and 2-m temperature anomalies compared with MERRA and National Oceanic and Atmospheric Administration (NOAA) station observations. The results first of all highlight the strong similarity between the two resolutions. This suggests that the coarser (1/2°) resolution is sufficient for addressing the impact of the SST anomalies, and we will take advantage of that fact by relying on 1/2° simulations to assess the impacts of the different ocean basins (see next section). The simulated precipitation anomalies show a distinct dipole structure over the eastern United States, with positive anomalies in the southeast and along the East Coast, and negative anomalies to the northwest extending from Texas, across the Ohio Valley, and into Canada. Weak positive anomalies occur along the Mexican Sierra Madre Occidental, and extending northward into New

[1] We focus on precipitation (in lieu of snow) because the model-simulated snow amounts are unrealistic.

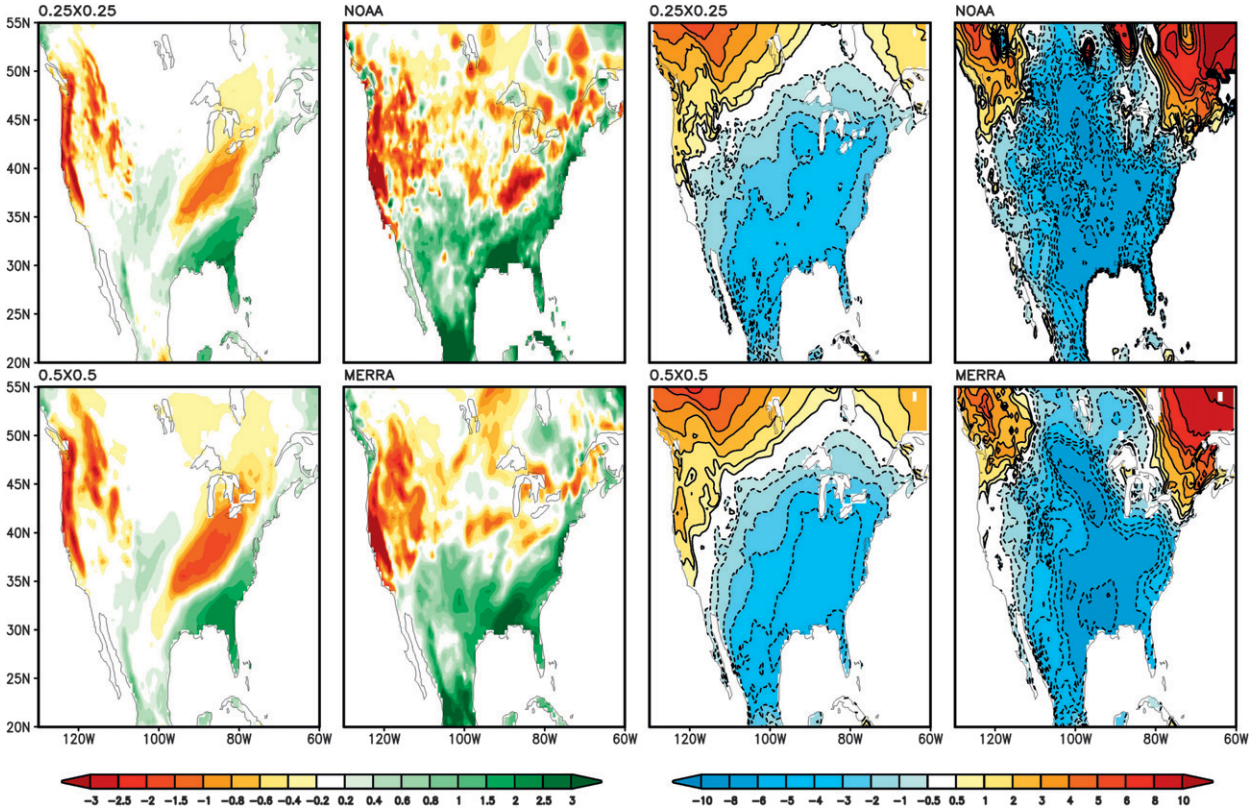

FIG. 4. (left two columns) Mean precipitation (mm day^{-1}) and (right two columns) T2m (°C) differences February 2010 − February 2000. The model results are based on an ensemble of 50 AGCM hindcasts: (top) 1/4° and (bottom) ½° resolution. The hindcasts were initialized (1 Dec 1999 and 1 Dec 2009). The hindcasts are verified by the (top) NOAA station observations and (bottom) MERRA reanalysis for the same periods.

Mexico and Colorado. Negative anomalies occur along the West Coast and the Rocky Mountains north of about 35°N latitude. All these features are, for the most part, consistent with the observations, though the observed anomalies are noisier and more widespread, and tend to be of larger amplitude (e.g., over Mexico). Again, this is likely in large part the result of the noise (unforced component) inherent in the observed anomalies.

The ensemble-mean surface temperature anomalies (Fig. 4) are characterized by negative anomalies over most of the United States, with the largest anomalies in the southern and eastern parts of the continent. Positive anomalies occur to the north, extending north and west from the Pacific Northwest, and over the northeast United States, extending north to cover the region east of the Hudson Bay. The observations are again very similar to the ensemble-mean results, though a region of pronounced negative anomalies in the upper midwestern United States extending into Canada is not evident in the simulations.

It should be emphasized that we are evaluating the differences between the two years, and those differences may not reflect the anomalies that occurred during the winter of 2009/10. In fact, an inspection of the observed February precipitation anomalies along the East Coast during those two years indicates some nonlinearity, in the sense that the differences reflect a positive anomaly in the southern tier and mid-Atlantic states during 2010, and a substantial negative anomaly in the Southeast during 2000. So that while the simulated difference fields appear to be realistic, it is not clear that the model is providing a realistic simulation of the storm activity that occurred during the individual years. We address that issue here by computing a more direct (compared to 250-mb v'^2) measure of storminess. The results (Fig. 5), based on daily surface pressure tendencies (following Hoerling 2010), show that the model simulates realistic storminess distributions as well as the changes that occurred along the Eastern Seaboard between the two Februaries, with enhanced storminess extending from the mid-Atlantic states northward during 2010, as well as a general southward shift in the Atlantic storm track. There are differences in the relative strength of the storminess in the two ocean basins, with MERRA showing larger values in the Pacific compared with the Atlantic (especially during 2000), while the model

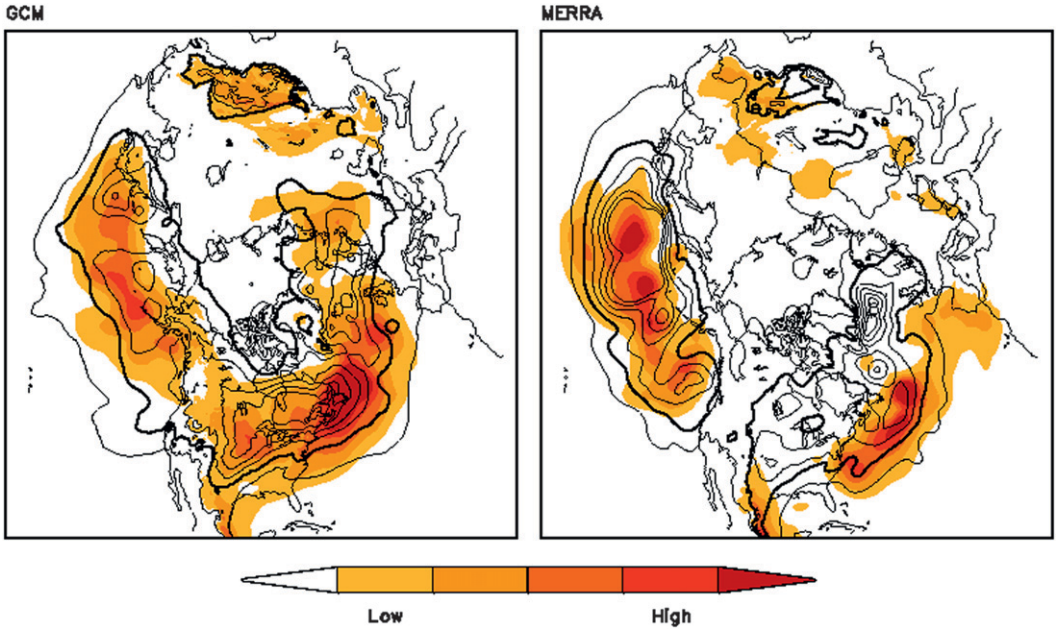

FIG. 5. The storm activity during February 2000 (contours) and February 2010 (shading). The fields consist of the variance of the daily surface pressure tendencies normalized by the Coriolis parameter (following Hoerling 2010). (left) Based on the two sets of 1/4° 50-member ensemble runs forced with observed SST and (right) from MERRA. The bold contours for 2000 correspond to the first shading level for 2010.

results indicate the opposite. This could in part reflect sampling uncertainties, since the MERRA results are, of course, for a single case.

We get a further sense of the nature of the changes in the weather statistics in Fig. 6, which shows the histograms of the daily precipitation and 2-m temperature (T2m) along the East Coast for the two Februaries (50 ensemble members each). The precipitation distributions show an increase in the probability of extreme precipitation events during 2010. For example, that the probability of getting a precipitation amount >10 mm day^{-1}, increased from 0.10 in February 2000 to 0.14 in February 2010; a 40% increase in the chance of such an extreme event. Also, the T2m distributions show a clear shift to colder values, changing from a distribution with a broad peak centered on about 7°C during 2000 to a distribution with a much sharper peak centered near 2°C during 2010.

The above-mentioned results suggest that the GEOS-5 AGCM, when forced with observed SST anomalies, produces quite reasonable February upper-tropospheric mean height, precipitation, surface temperature, daily upper-level v wind variance, and storminess differences between the two winters. While we have not ruled out the possibility that model deficiencies account for some of the discrepancies between the ensemble mean and observed fields, we will show evidence (in section 3c) that suggests that much of the difference is because the observed anomalies include a significant noise component that is largely removed from the simulations by the calculation of ensemble means. We will, however, first examine a number of other experiments (all run at ½° horizontal resolution) that attempt to isolate the impact of the North Atlantic and Indian Ocean SST anomalies from the impact associated with the SST anomalies in the Pacific basin.

b. *Isolating the impacts of the Pacific, North Atlantic, and Indian Ocean SSTs*

While ENSO (and presumably the associated Pacific SST anomalies) is clearly playing a major role in the model response, we next attempt to isolate the impact of the North Atlantic and Indian Ocean SSTs from that of the Pacific SST.[2] We do this by rerunning the experiments for the two winters but, in these runs, the SSTs in the basin of interest are switched between the two winters. In particular, we examine the separate impacts of the North Atlantic (between 10°S to 75°N) and Indian Oceans. The results of those runs (together with those

[2] Here, we do not imply that the SST anomalies in the Indian and Atlantic Ocean basins are completely unrelated to ENSO.

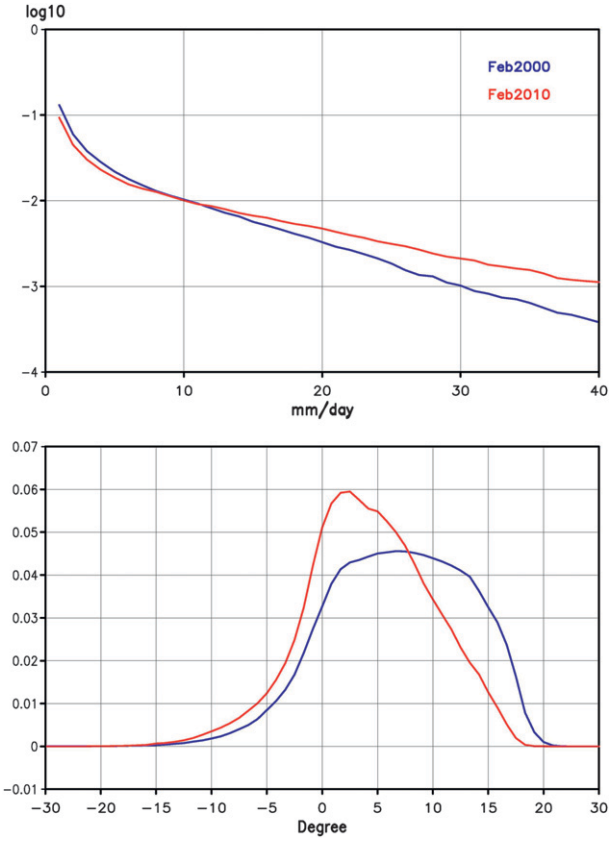

FIG. 6. The normalized histograms of (top) precipitation (note the log scale) and (bottom) T2m for February 2000 and February 2010. The results are based on the two sets of 1/4° 50-member ensemble runs forced by the observed SST, using daily values of the precipitation and T2m averaged over the region (30°–45°N, 85°–75°W).

run with observed SST) allow us to isolate the impact of the SST (see Table 1) as:

$$\mathrm{NAtl}_{2000} = (C - A), \tag{1a}$$

$$\mathrm{NAtl}_{2010} = (B - D), \tag{1b}$$

$$\mathrm{Ind}_{2000} = (E - A), \quad \text{and} \tag{1c}$$

$$\mathrm{Ind}_{2010} = (B - F), \tag{1d}$$

where, for example, NAtl_{2000} indicates that we are estimating the impact of the North Atlantic SST based on two sets of 50 runs forced with the observed 1999/2000 SST everywhere except in the North Atlantic, where run C has the SST from the 2009/10 winter. Similarly, NAtl_{2010} indicates that we are estimating the impact of the North Atlantic SST based on two sets of runs forced with the observed 2009/10 SST everywhere except in the North Atlantic, where run D has the SST from the 1999/2000 winter.

We can also take advantage of various other combinations of the runs to obtain estimates of the overall impacts of the different ocean basins (Pacific, North Atlantic, Indian Ocean) as

$$\mathrm{NAtl} = 1/2[(B - A) + (C - D)], \tag{2a}$$

$$\mathrm{Ind} = 1/2[(B - A) + (E - F)], \quad \text{and} \tag{2b}$$

$$\mathrm{Pac} = 1/2[(D - C) + (F - E)]. \tag{2c}$$

Note that

$$B - A = (\mathrm{Pac} + \mathrm{Ind}) + \mathrm{NAtl} = (\mathrm{Pac} + \mathrm{NAtl}) + \mathrm{Ind}, \tag{3a}$$

$$(\mathrm{Pac} + \mathrm{Ind}) = 1/2[(B - A) + (D - C)], \quad \text{and} \tag{3b}$$

$$(\mathrm{Pac} + \mathrm{NAtl}) = 1/2[(B - A) + (F - E)]. \tag{3c}$$

Each of the following eight panel figures have the same format, showing the total difference and the various combinations defined in (1) and (2). Figure 7, for example, shows the global results for the 2-m temperature. It highlights the dominance of the Pacific SST (shown in Fig. 7c) in forcing the temperature changes (Fig. 7a) over North America and most of the other land areas (cf. Figs. 7c,e,g). Over the ocean, the results are, of course, highly constrained by the imposed SST, but here the plots serve to summarize the spatial distribution of the SST forcing in the various experiments. Figures 7b,d,f,h show that the responses to the Indian and North Atlantic SSTs tend to be somewhat more local, but the SST in both ocean basins does have an impact on North America. There are also some interesting nonlinearities in the responses (there are differences in the responses between 2000 and 2010), and we will discuss those later in our focus on the U.S. East Coast.

Figure 8 shows the responses in the February 250-hPa height anomalies. Figure 8a can be compared with the top left panel of Fig. 2 to see the impact of resolution on the height response. The results for the two resolutions are overall very similar with the largest differences confined to the Arctic region, where the intraensemble variance is largest (see Fig. 12). The upper-level response is, to a large extent, controlled by the Pacific SST (Fig. 8c). There are small contributions from the North Atlantic (Fig. 8e) and the Indian Ocean (Fig. 8g), with the latter showing an AO-like response that is consistent with previous studies of the impact of the Indian Ocean SST (e.g., Hoerling et al. 2004). Figures 8b,d illustrate

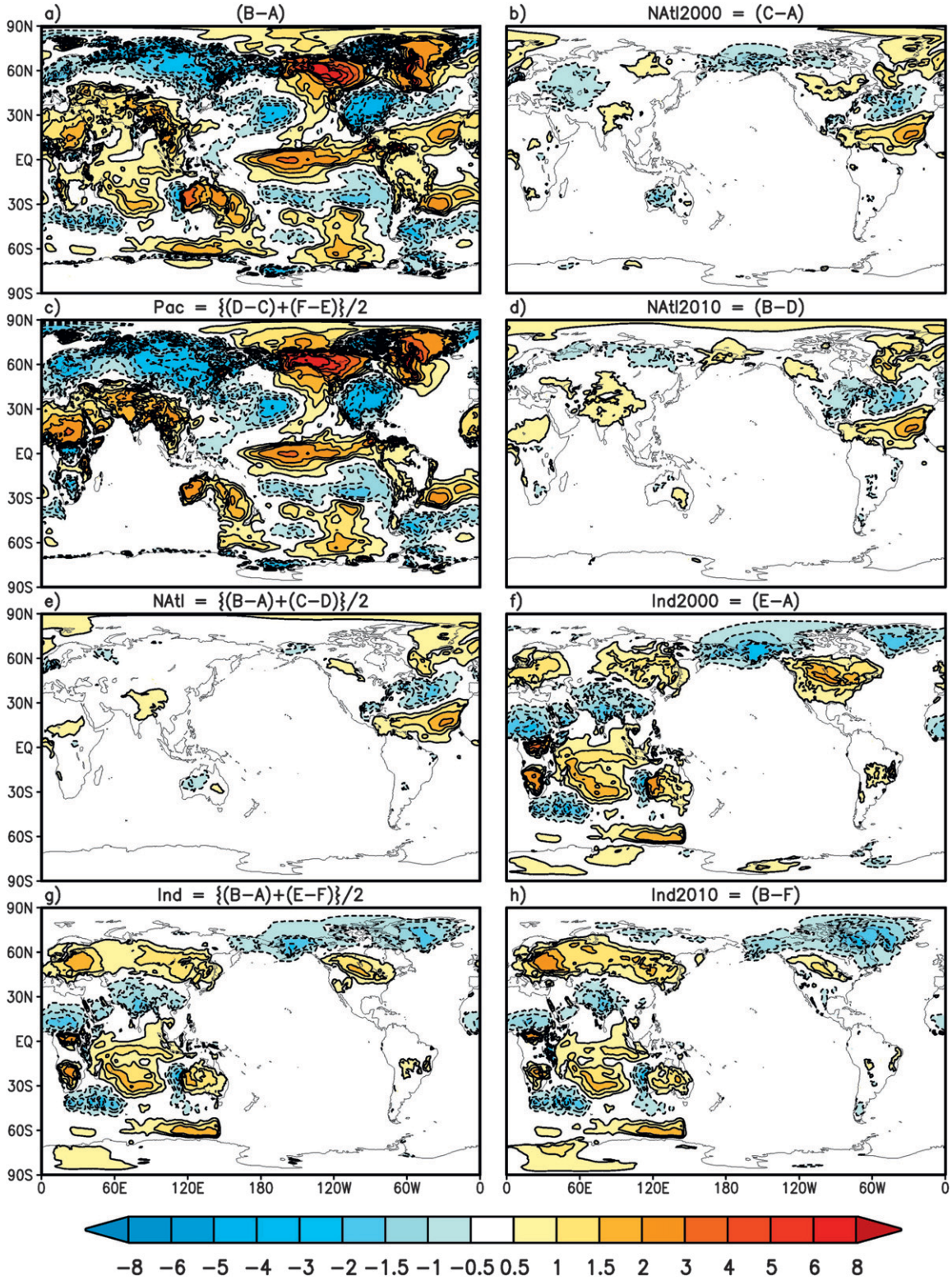

FIG. 7. Estimates of the impacts of SST forcing from the different ocean basins on T2m (°C). Results are shown for the ensemble-mean February differences. The letters refer to the runs listed in Table 1. (a) The impact of the observed SST: Feb 2010 − Feb 2000 (B − A). (b) The impact of the North Atlantic SST during 2000: (C − A). (c) The impact of the Pacific Ocean SST: ½(D − C + F − E). (d) The impact of the North Atlantic SST during 2010: (B − D). (e) The average impact of the North Atlantic SST: ½(B − A + C − D). (f) The impact of the Indian Ocean SST during 2000: (E − A). (g) The average impact of the Indian Ocean SST: ½(B − A + E − F). (h) The impact of the Indian Ocean SST during 2010: (B − F).

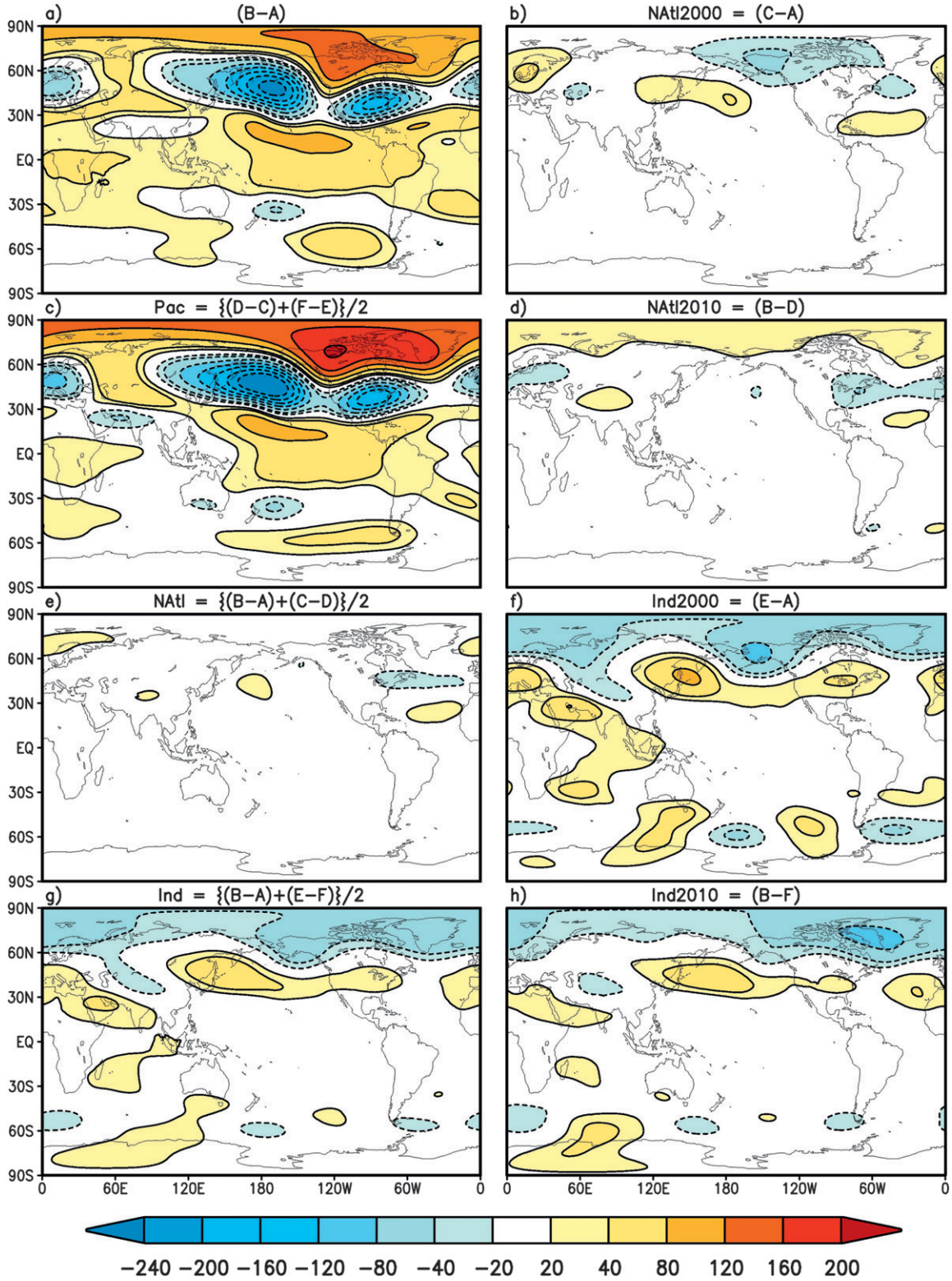

FIG. 8. As in Fig. 7, but for 250-mb height (m).

how the impact of the North Atlantic SST depends to some extent on the SST in the other ocean basins. In particular, the impact has a much more AO-like structure in the presence of the 2009/10 SST (an El Niño winter). The far-field impacts are to some extent of opposite sign in the two winters, so that the average response (Fig. 8e) is small everywhere except over the Atlantic. In the case of 2010, the response shows a negative height anomaly extending over the U.S. East Coast (Fig. 8d) that, as we shall see later, plays a role in the propensity for snowstorms that year. The Indian Ocean impact during 2010 is primarily to counteract the high-latitude response to the Pacific SST and to contribute to the overall slight weakening of that response (cf. Figs. 8a,c).

The impacts on the submonthly 250-hPa v wind variance are shown in Fig. 9. As noted previously, the total difference field (Fig. 9a) has a band of enhance variance that extends from the subtropical eastern North Pacific, and across Mexico, the southern United States, and southern Eurasia. Major regions of reduced variance occur just to the north, extending from the North Pacific across North America into the North Atlantic, and across northern Eurasia. The above-mentioned changes, as well as those in the Southern Hemisphere, suggest an overall southward shift in the midlatitude submonthly transients in both hemispheres. These changes are to a large extent forced by the Pacific SST (Fig. 9c). The impacts of the other ocean basins are considerably smaller. The impact of the North Atlantic is to contribute to the southward shift of the transients over Europe—especially during 2010 (Fig. 9d). The impact of the Indian Ocean SST is to enhance the variance in the southern Indian Ocean (Fig. 9g), and parts of the eastern Pacific of both (Northern and Southern Hemispheres), and to reduce the variance across much of the rest of the Northern Hemisphere. The impact is generally larger for 2000 than for 2010 (cf. Figs. 9f,h).

We next return to the impact on the United States. Figure 10 shows the impact on 2-m temperature. We see that most of the basic difference pattern over the United States is forced by the Pacific SST. The Pacific-forced cooling is in fact larger than the total change (cf. Figs. 10a,c) over much of the northern and central parts of the country. This cooling is counteracted in part by warming from both the North Atlantic and Indian Oceans (Figs. 10e,f), though for the North Atlantic that reflects primarily the response for 2000 (Fig. 10b). The North Atlantic also acts to contribute to the cooling along the East Coast. This is largely the result of the impact during 2010 (Fig. 10d), with 2000 showing a slight warming along the East Coast. The Indian Ocean also shows considerable differences in the impact between the two winters, with warming over the entire country during 2000 (Fig. 10f) and some cooling along the southern states and along the East Coast during 2010 (Fig. 10h).

Figure 11 shows the impact of the SST in the different ocean basins on U.S. precipitation. Here again, the Pacific SSTs dominate the response with positive anomalies along the southern and eastern parts of the country, and with reduced precipitation in the Pacific Northwest and from Texas northeastward through the Ohio River valley. The impact of the Indian Ocean and North Atlantic SST is primarily to reduce further the precipitation throughout the Ohio River valley. During 2010, both basins also contribute to the—primarily Pacific forced—precipitation enhancements in the Southeast.

In summary, the model results show that the main differences between the two Februaries are forced by the Pacific SST anomalies associated with ENSO (La Niña in 2000 and El Niño in 2010). This includes the basic PNA-like upper-level height anomalies spanning the North Pacific, North America, and the North Atlantic, and the submonthly meridional wind variances that include a band of enhanced variance extending from the eastern subtropical North Pacific, across the southern United States, the North Atlantic, and southern Eurasia. The impacts of the other ocean basins are secondary, with notable impacts from the North Atlantic SST during 2010 consisting of enhanced cooling along the U.S. East Coast and an enhancement (reduction) of meridional wind variance across southern (northern) Europe. The exact mechanism by which the North Atlantic SST impact the temperature and precipitation over the United States is not clear, though it appears to be linked to the height field response that extends westward across the eastern half of the continent, forcing changes in the low-level temperature and moisture advection. The basic response to the Indian Ocean SST differences (enhanced warmth) is a positive AO-like response that keeps cold Arctic air from extending as far south into North America (compared with the negative phase), keeping much of the United States warmer than normal. At upper levels, the positive AO response counteracts the high-latitude ENSO impact.

We next turn to the issue of predictability with a focus on the intraensemble variance.

c. *Predictability*

It was mentioned earlier that some of the differences that we see between the ensemble mean and the observed February fields (e.g., Fig. 2) may be due to internal atmospheric noise associated with the unforced component of atmospheric variability. We can estimate the noise component from the interensemble variance

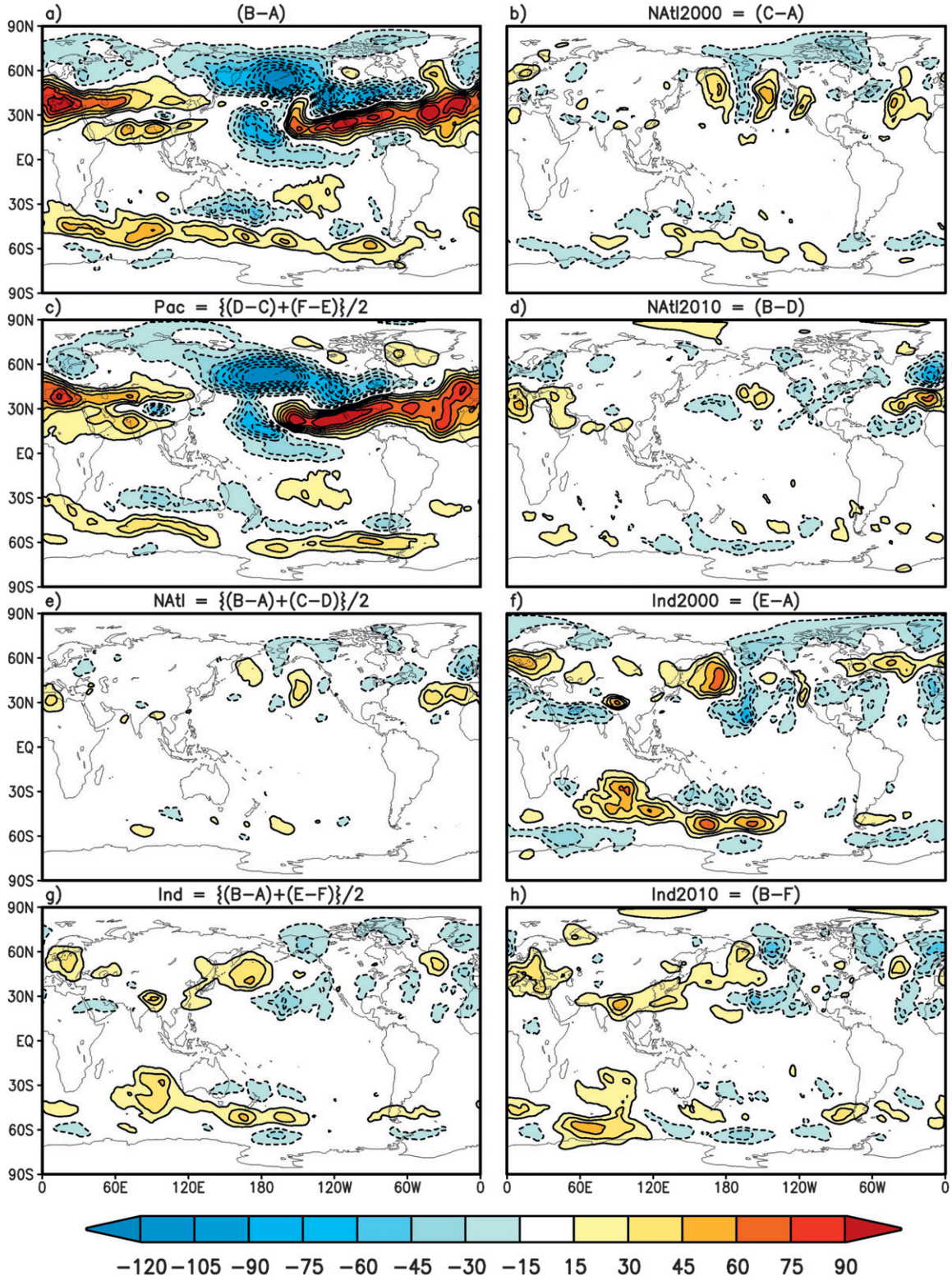

FIG. 9. As in Fig. 7, but for 250-mb daily transients (v'^2, m^2).

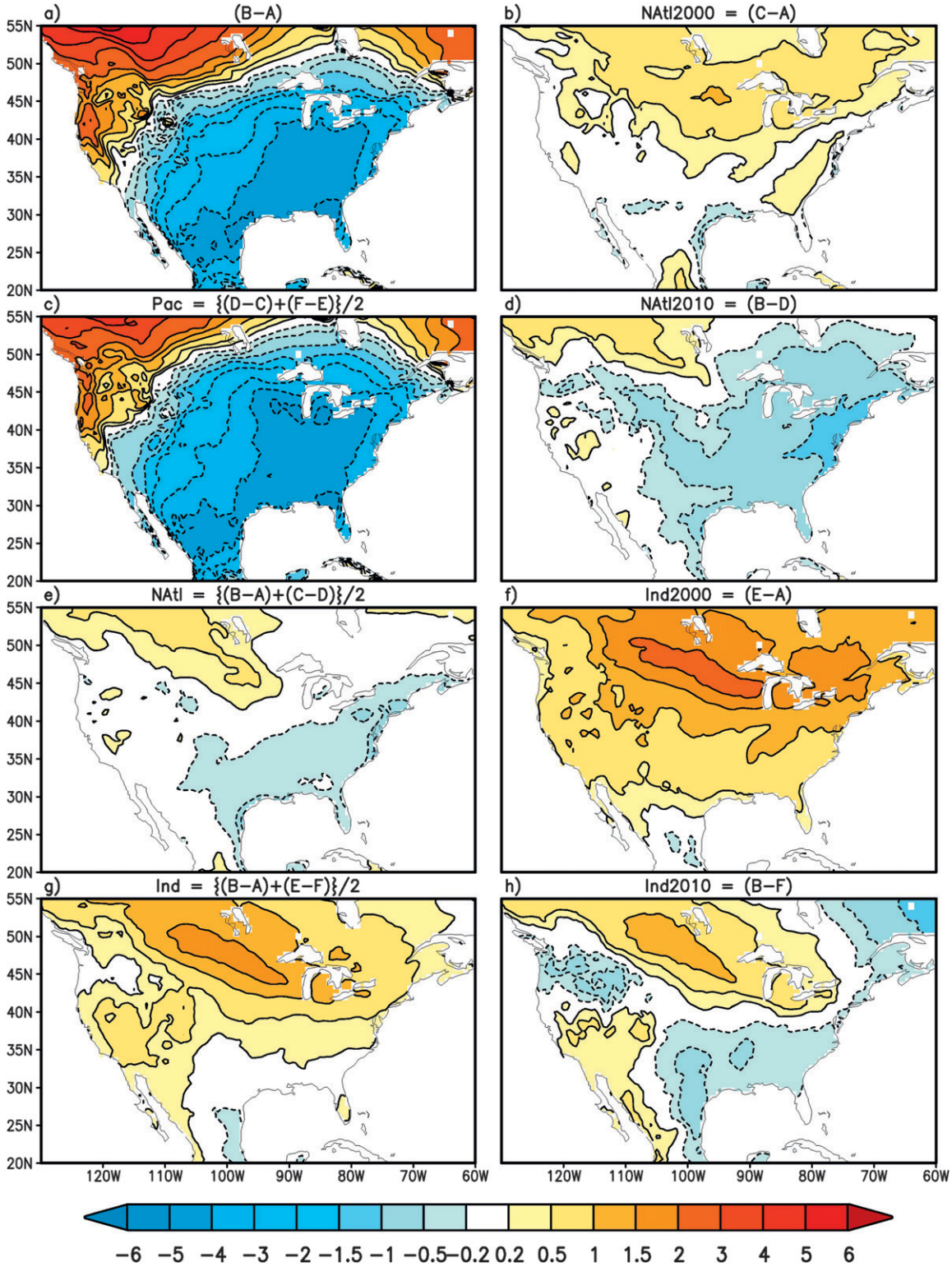

FIG. 10. As in Fig. 7, but for T2m (°C) over the United States.

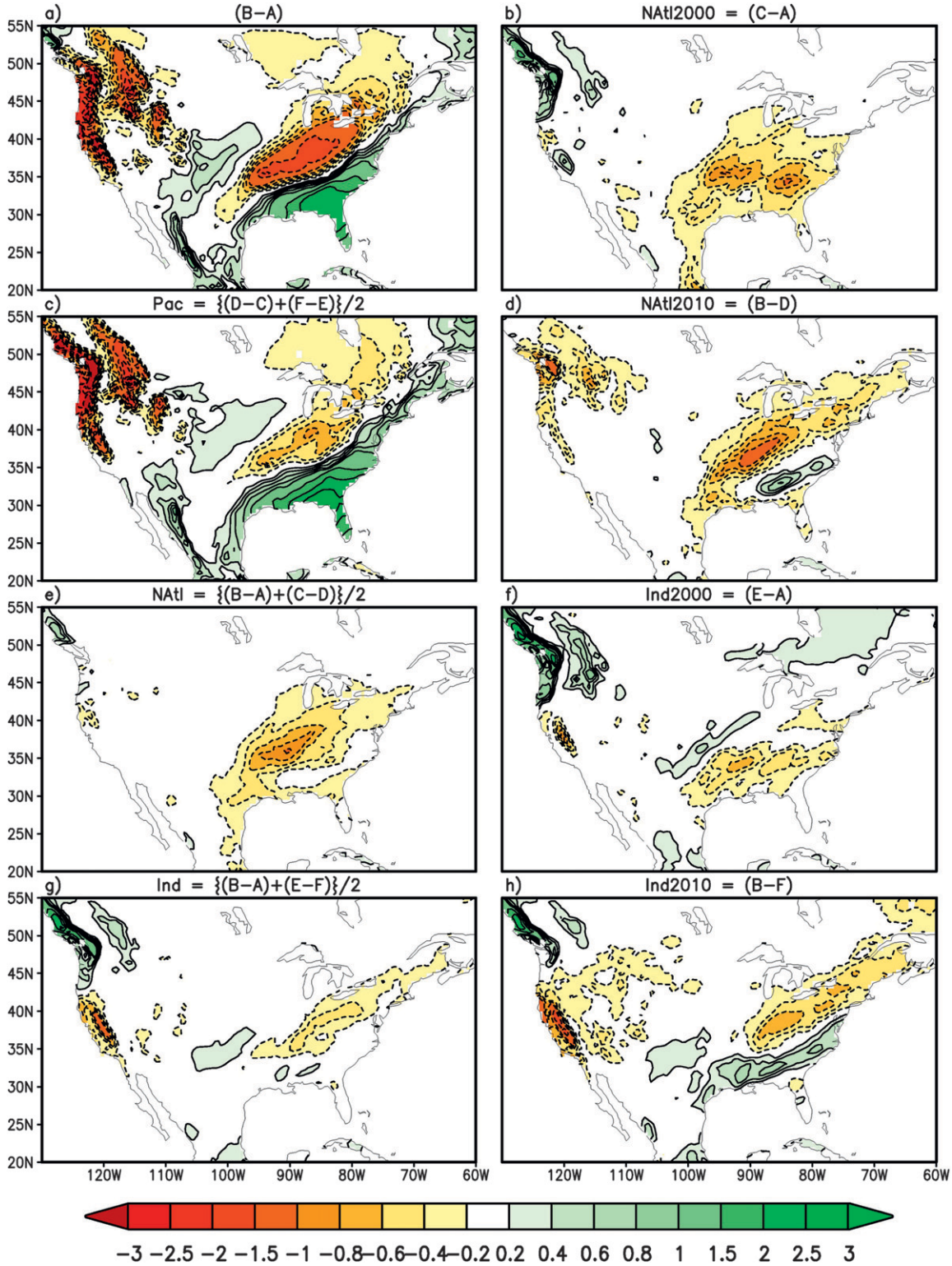

FIG. 11. As in Fig. 7, but for precipitation (mm day^{-1}) over the United States.

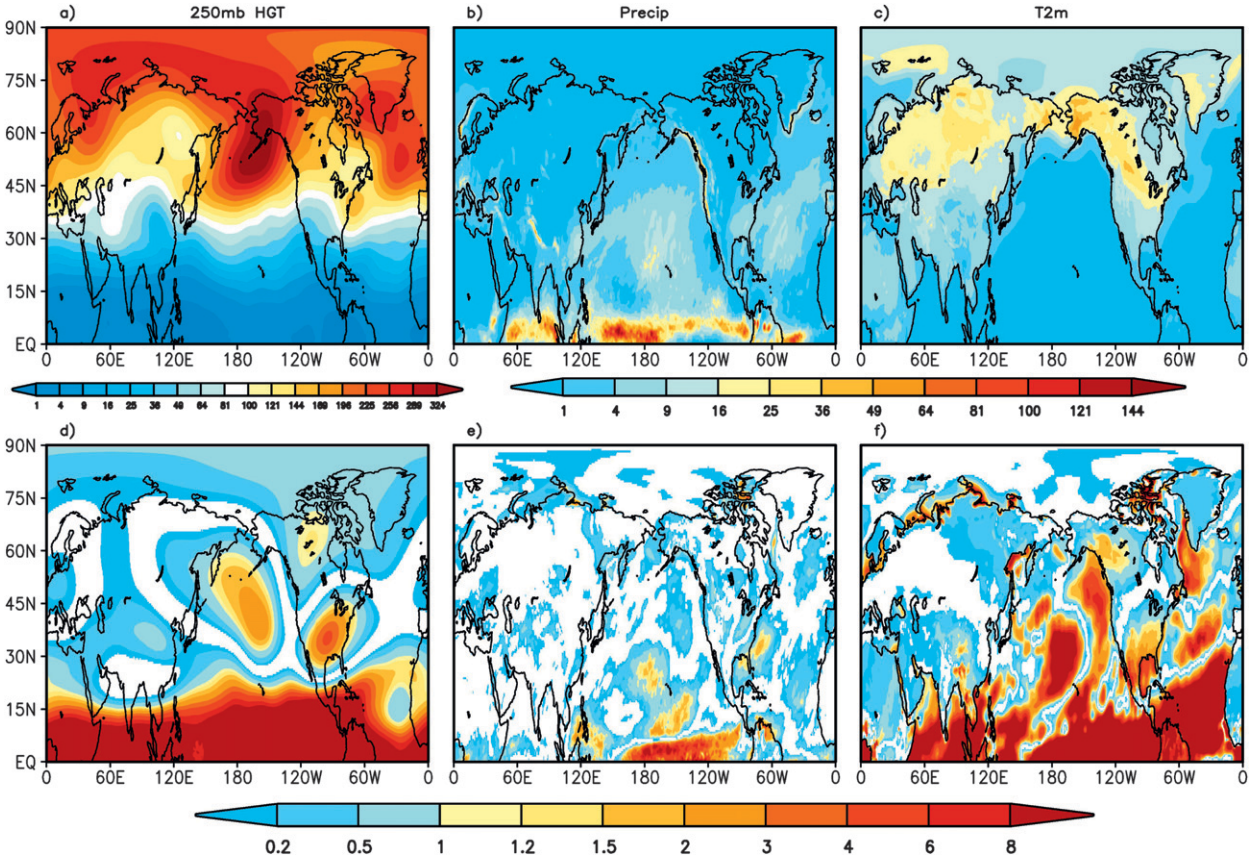

FIG. 12. (top) Intra-ensemble variance of the (February 2010 − February 2000) differences for 250-mb height (m^2) precipitation (mm day^{-1}), and T2m ($°C^2$). (bottom) As in (top), but for the S/N of the differences. White areas in the S/N fields indicate where the difference fields are not significantly different from zero based on a one-sided *t* test at the 0.5% level.

based on the 50 ensemble members for each set of runs. Figure 12a shows, for example, the intra-ensemble variance of the February 250-hPa height differences based on the two sets of ½° runs, computed as

$$N = \overline{(\Delta - \overline{\Delta})^2}. \tag{4}$$

Here Δ is the difference (2010 minus 2000) between any two February means, and the overbar is an ensemble average. The figure shows that the largest height variance occurs, as expected, in the mid- and high latitudes. The variance is largest in the North Pacific, the eastern North Atlantic, Europe, and the Arctic, with the lowest midlatitude variance occurring over central Canada, eastern North America, and central and eastern Asia. Figure 12b shows that the precipitation variance is largest in the tropics associated with the ITCZ. Other regions of locally enhanced precipitation variance include the central North Pacific and a region extending from the eastern United States across the North Atlantic. The T2m variance (Fig. 12c) is largest over the high latitudes of the interior continents and over Alaska. Over the United States, the largest variance occurs over the upper Midwest and the region extending westward to the East Coast.

Figure 12d shows the signal-to-noise (S/N) ratio of the February 250-hPa height differences, computed as

$$\mathrm{S/N} = \frac{\overline{\Delta}^2}{\overline{(\Delta - \overline{\Delta})^2}}. \tag{5}$$

The highest S/N occurs again, not surprisingly, in the low latitudes. Outside the tropics there are distinct regions with locally enhanced S/N. These include the central North Pacific, northern Canada, and the eastern United States. Figure 12e shows the S/N for the precipitation. Here, the largest values occur in the central tropical Pacific (associated with ENSO), with other regions of enhanced S/N occurring over the subtropical central North Pacific and the Eastern Seaboard of the United States, suggesting some predictability in the region of the snow storms. The S/N for the T2m (Fig. 12f) is largest

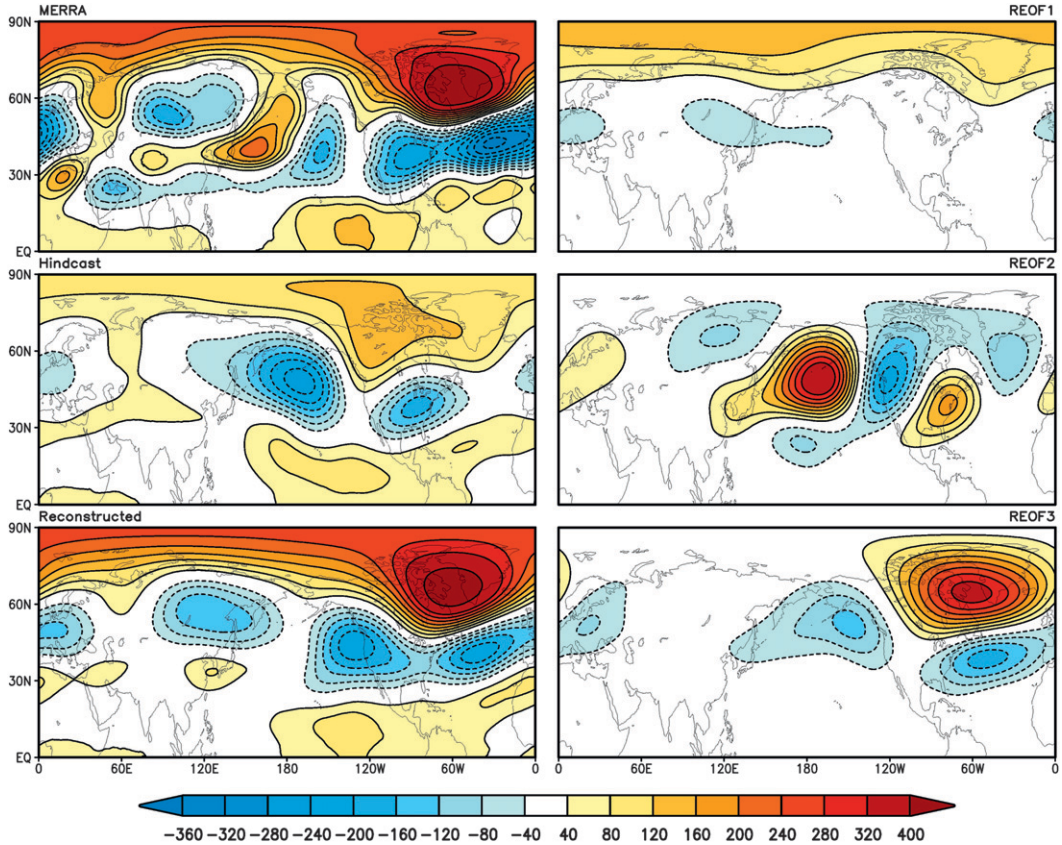

FIG. 13. (top to bottom) (right) The three leading REOFs of the 250-mb intra-ensemble variance, computed from monthly (February) model data. The weightings of the three leading REOFs are all negative (−30.9, −70.4, −65.6) and are determined from a linear regression that fits the (top left) MERRA difference field as a linear combination of the three REOFs plus (middle left) the model ensemble mean difference. (bottom left) The results of the fit to the observed difference field. See text for details. Units are m.

over the tropics and central subtropical Pacific, with values exceeding 8 is some regions. Other regions with a S/N larger than one occur off the west coast of North America, the southeastern United States extending north to Washington, D.C., and parts of the North Atlantic (just off the East Coast of the United States and over the Labrador Sea).

The above-mentioned results suggest that the high noise variance in the North Pacific can account for the large differences we see between the ensemble mean and the reanalysis (Fig. 2). Similarly, the much larger anomalies in the North Atlantic in MERRA compared with the ensemble mean (Fig. 2) may simply reflect the substantial noise component in that region. To quantify that, we attempt to reconstruct the MERRA height difference field as a linear combination of the model's ensemble mean and the leading noise components. Here, we compute the noise components based on a rotated empirical orthogonal function (REOF; Richman 1986) decomposition of the February intraensemble variance computed from all the model experiments.[3] The first three REOFs (right panels of Fig. 13)[4] account for 16%, 10%, and 10%, respectively, of the total intra-ensemble variance. The leading REOF (top right panel of Fig. 13) resembles the AO, while the second has a PNA-like structure, and the third resembles the NAO. Using those three REOFs (E_1, E_2, E_3) as predictors, we form the following regression equation:

$$\Delta_{\mathrm{Obs}} = \overline{\Delta}_{\mathrm{Model}} + \alpha E_1 + \beta E_2 + \gamma E_3 + \varepsilon, \qquad (6)$$

[3] This includes all the ½° experiments listed in Table 1 plus four other sets of (50 ensemble members) experiments (not discussed) that consist of switching just the tropical Atlantic SST and running with the North Atlantic SST replaced by the average of the 2 yr, for a total of 10 × 50 = 500 Februaries.

[4] We note that we have adopted the usual sign convention of the AO, PNA, and NAO, so that the patterns shown on the right-hand side of Fig. 13 represent the negative phases of these patterns (and a negative weighting of the REOFs).

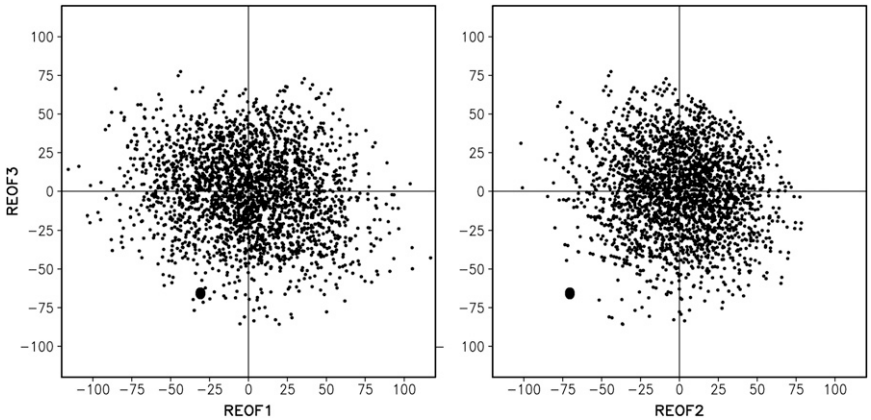

FIG. 14. A scatterplot of the 50^2 differences between the leading rotated principal components or RPCs of the intransemble variance (based on the February 250-mb height REOFs) for 2010 and 2000. The *y* axis is for RPC 3 and the *x* axis is for (left) RPC 1 and (right) RPC 2. The large dot in each panel indicates the values obtained from the regression that fit the noise REOFs to the observed difference fields (see Fig. 13).

where ε is a residual and α, β, and γ are the regression parameters. The bottom left panel of Fig. 13 shows the results of minimizing ε^2 over the Northern Hemisphere ($\alpha = -30.9$, $\beta = -70.4$, $\gamma = -65.6$). The results show that one can—to a good approximation—reproduce the observed difference field with the ensemble mean and just the three leading noise REOFs. Some notable differences between the observed and reconstructed differences are the shortwave structure over eastern Asia and the North Pacific that is in MERRA but not the reconstructed field, and the very large amplitude negative NAO structure in the MERRA difference that is not fully reproduced in the reconstructed field.

It may, of course, be that the differences between the observed and reconstructed fields to some extent reflect model errors. This is suggested by Fig. 14, which shows that the amplitudes of the PNA and NAO noise REOFs [the second and third rotated principal components (RPCs)] needed to fit to the observed differences are very near to the most extreme values actually realized by the model ensembles.

We address that possibility more directly here, by examining whether the observed difference fields fall outside the range of the model's probability distribution of the difference fields. We determine the model's probability density function of the difference fields at each grid point, by considering all 50^2 combinations of the two (2010 and 2000) sets of 50 ensemble members. Figure 15 shows that there are indeed regions where the observed difference (from MERRA) is a rare occurrence in the model world. This includes a substantial part of the tropics and the local extremes, located primarily in the centers of the troughs and ridges. We point out, in particular, the NAO-like north–south dipole in the North Atlantic that is at the edge of—if not beyond—the model's range of noise variance. The latter suggests that some of the discrepancy between the observed and ensemble-mean response in the North Atlantic difference may be due to model deficiencies in reproducing that feature (e.g., insufficient forced response or insufficient intraensemble variance). Conversely, we have chosen this event because it is extreme in nature, and this result may in fact be consistent with it being a chance extreme occurrence of the noise (unforced) NAO pattern that develops in conjunction with the SST-forced component.

In the case of the PNA, in addition to having large amplitude, the negative phase is opposite of the observed index (the comparison here is made with the monthly-mean observed PNA indices based on the modified pointwise estimate as described in http://www.cpc.ncep.noaa.gov/products/precip/CWlink/pna/month_pna_index2.shtml). This discrepancy could again be due to model errors, but it could also be the result of an observed index that reflects a mixture of the El Niño response and the PNA. Evidence for this is the fact that the observed PNA index remains large and positive for much of the 2009/10 winter, something that is unlikely if it were to only reflect the unforced (internally driven) PNA in view of its much shorter intrinsic time scale (<10 days; Feldstein 2000). In fact, if we compute a simple pointwise PNA index based on the full February differences of the individual ensemble members (rather than first removing the ensemble mean), we do indeed find that it is predominantly positive. While it can be argued that the PNA is itself directly forced by the El Niño, there is considerable evidence that this does not occur (Straus and Shukla 2002).

Despite these caveats about the leading simulated noise patterns, it does appear that the unforced component of

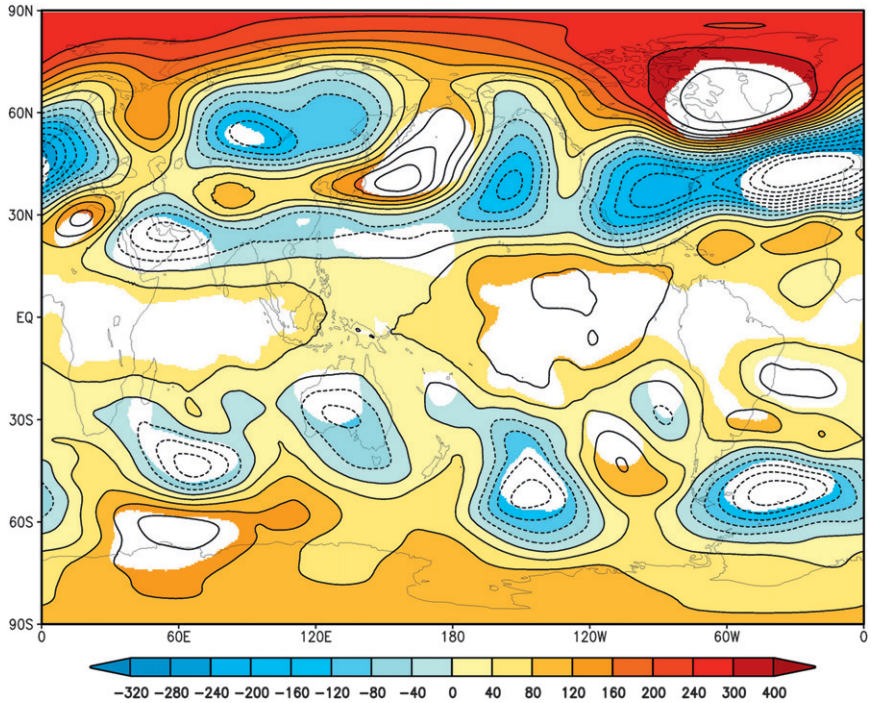

FIG. 15. The 250-mb height difference (m) (February 2010 − February 2000) from MERRA. The unshaded regions are where the MERRA difference value falls outside the 90% confidence interval (<5% or >95%) of the model difference values. The model confidence intervals are estimated from the 50 ensemble members from each year. See text for details.

the flow plays an important role in the observed height anomaly patterns. Estimates of the impact of the noise components of the flow on surface meteorology are summarized in Fig. 16, which shows the correlations and covariances between the leading 250-mb height noise PCs and the precipitation and surface temperature. The covariances are normalized to reflect the changes in precipitation or T2m associated with a one standard deviation (std dev) change in each REOF (with the sign changed to indicate the sense of the impact during 2010). The correlations for all three PCs are in general modest, though both the PNA and NAO have areas of significant correlations over the eastern United States (with magnitudes in some regions >0.4). The negative phase of the PNA is associated with an increase in precipitation (>0.4 mm day^{-1} with a one std dev change in the PC) over much of the interior eastern United States, west of the Appalachian mountains, while the negative phase of the NAO acts to reduce the precipitation over the eastern United States, especially over the mid-Atlantic states (>0.4 mm day^{-1} with a one std dev change in the PC). The negative NAO is also linked to cooling along the East Coast (>0.5° with a one std dev change in the PC), while the negative PNA is associated with warming over much of the eastern United States (>1° with a one std dev change in the PC). The AO appears to have little connection to the precipitation or temperature over the eastern United States, with however significant impacts on the temperature over the upper Midwest and Canada.

The above-mentioned results provide estimates of the *potential* contributions of the noise to the precipitation and T2m differences. The reader is cautioned, however, in drawing any conclusions about the *actual* contributions of the three noise REOFs to the 2010 − 2000 differences in the precipitation and T2m fields. Unlike for the height field, here, the linearity assumption appears to break down, in the sense that summing the ensemble mean and the appropriately weighted noise contributions (based on the above-mentioned covariances), does not reproduce the observed changes in these fields. Nevertheless, the fact that both the PNA and NAO had unusually large amplitudes and that they appear to impact both precipitation and temperature over the eastern United States indicate that a full accounting of the causes of the unusual snowstorm activity must include an assessment of the nature of the unforced (noise) component of the flow. Whether the large ''noise'' component of the flow is a truly unpredictable random occurrence or whether it is influenced by mechanisms

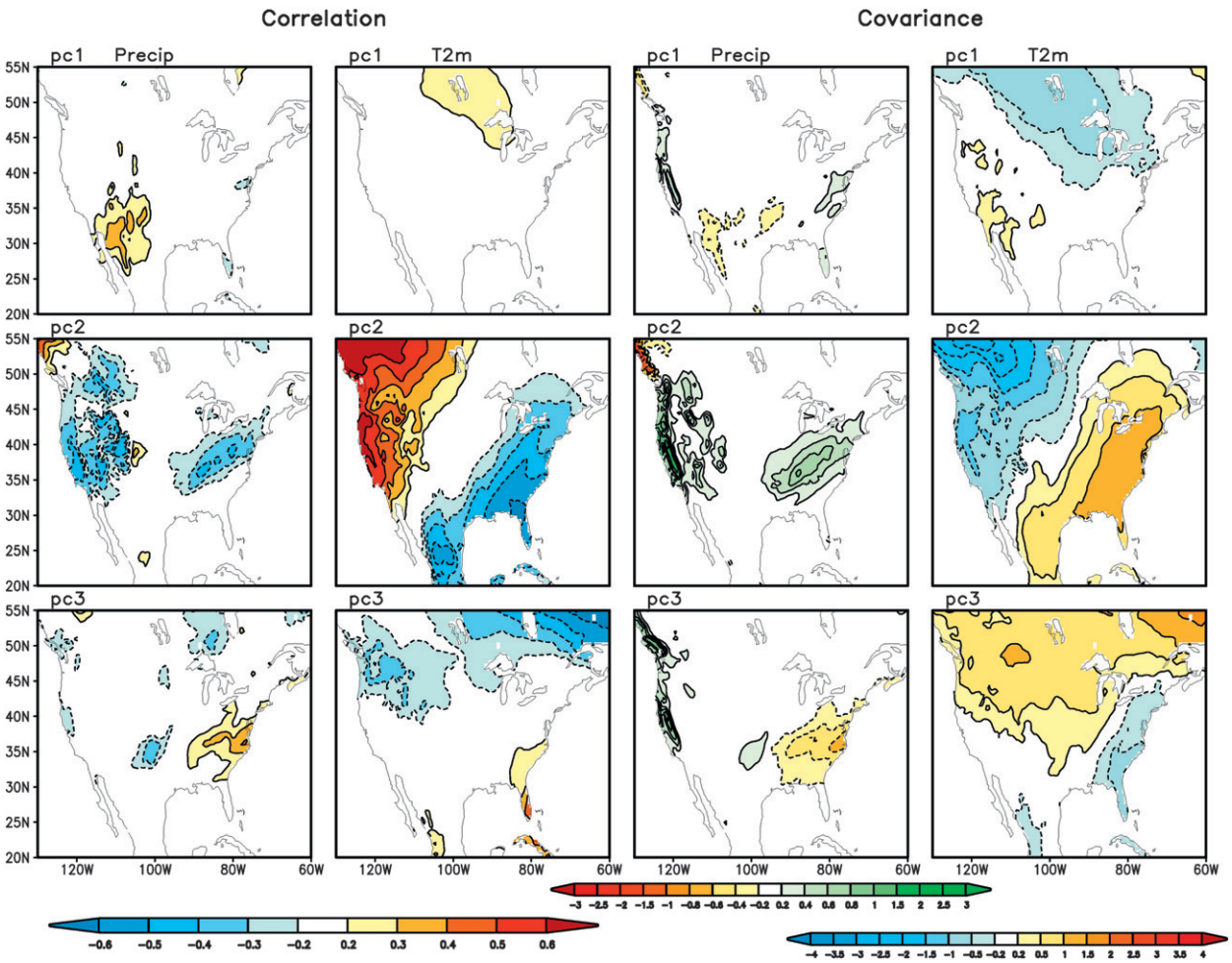

FIG. 16. (left two columns) The correlation between the three leading noise PCs and the precipitation and T2m, respectively. (right two columns) As in (left), but for the negative covariance between the precipitation (T2m) and the PCs, normalized by the standard deviation of the PCs. Results are based on the February monthly-mean noise (intra-ensemble variance) computed from the 50-member ensemble runs with observed SST for the years 2010 and 2000. With 100 ensemble members, a correlation coefficient of 0.2 is significantly different from 0 at the 5% level, based on a *t* test. Units for the normalized covariances are mm day^{-1} and °C (reflecting the changes associated with a one standard deviation change in the PCs).

not addressed here is still an open question (see next section).

4. Summary and conclusions

The extreme U.S. East Coast snowstorm activity of the 2009/10 winter occurred at a time of a mature El Niño, a persistent negative North Atlantic Oscillation (NAO), and a warm Indian Ocean. A number of early assessments of the reasons for the unusual storm activity have focused on the relative roles of ENSO and the NAO (e.g., Seager et al. 2010; Hoerling 2010). Those (primarily statistically based) studies concluded that it was the unusual, persistently negative phase of the NAO that contributed more to the 2009/10 storms than the El Niño event, though both El Niño and the NAO have been historically linked to increased East Coast snowstorm activity. This study reexamines the cause(s) of the snowstorms, taking a modeling approach aimed at providing a quantitative assessment of the impacts of the prevailing SST anomalies, and giving further insights into the nature of the El Niño and the NAO impacts on the storm activity.

The study employed relatively large (50 members) ensemble, high-resolution simulations with the GEOS-5 AGCM forced with specified observed or idealized SST and initialized on 1 December. The focus was on assessing the impacts of the Pacific, Atlantic, and Indian Ocean SST anomalies. This was done by comparing the 2009/10 winter with another winter (1999/2000) that is

characterized by SST anomalies that are largely of opposite sign. It was shown that the observed SST force global-scale anomalies (defined as the ensemble-mean difference between February 2010 and February 2000) in the upper-level height field, precipitation, and surface temperature that are largely consistent with the observed anomalies. In particular, the model produces positive precipitation and cold temperature anomalies along the southeastern and East Coast of the United States, reflecting a propensity for enhanced snowstorm activity. It was further shown that this is part of a global-scale response in which the storminess is enhanced from the central subtropical North Pacific, across the southern United States (and the East Coast), the North Atlantic, and across southern Eurasia, with reduced storminess to the north of these regions—results that are consistent with the findings of Seager et al. (2010).

A number of additional experiments were carried out that attempt to isolate the roles of the North Atlantic, Pacific, and Indian Ocean SSTs. The basic results of those experiments indicate that the ensemble-mean temperature and precipitation anomalies over the United States are primarily driven by the ENSO-related Pacific Ocean SST. The impact of the North Atlantic SST is to contribute to the cooler temperatures along the U.S. East Coast, as well as to extend the Pacific-forced storminess anomalies eastward into Eurasia. The response to the Indian Ocean SST is an Arctic Oscillation–like pattern (see also Hoerling et al. 2004) that largely acts to counteract the response to the Pacific Ocean SST at mid- and high latitudes.

The issue of predictability was addressed in the context of the contribution of the unforced intraensemble variability or noise to the observed anomalies. It was found that 1) there is a large noise component to the observed upper-tropospheric height anomalies over the Northern Hemisphere and that 2) the observed anomalies are, in fact, well reproduced by the sum of the ensemble mean and the three leading modes of intraensemble variability. A key result concerning the role of the NAO is that one of the leading noise modes (the third) has an NAO-like structure that contributes substantially to the reconstruction of the observed anomalies in the North Atlantic. The observed NAO anomaly can therefore be considered to be composed of the following three components: 1) a noise component that dominates the anomaly, 2) a smaller but significant part that is directly forced by the Pacific SST, and 3) another yet smaller contribution occurring as a response to the North Atlantic SST. As such, the question of whether it was primarily ENSO or the NAO that produced the unusual storm activity is difficult to answer, since the response to the Pacific SST (by extending into the North Atlantic) itself has a substantial projection onto the NAO. Similar issues concern the role of the PNA, which contributed substantially to the noise in the simulations, but which observational estimates have difficulty separating from the ENSO response.

What we can say about the NAO-versus-ENSO issue from these experiments is that the Pacific SSTs are the main forcing of the predictable part of the anomalous storm activity. Despite the large noise component of the observed height anomaly over the North Atlantic, the main region of interest directly along the East Coast of the United States is relatively less influenced by the noise and is in fact characterized by some of the largest signal-to-noise ratios anywhere in the subtropical–middle latitudes (with values exceeding 3). The signal-to-noise ratios of the temperature and precipitation are more modest (exceeding 1 in that region), but nevertheless suggest a potential for predicting the unusual storm activity along the U.S. East Coast several months in advance.

There are some uncertainties in the results associated with possible model deficiencies, as well as the design of the experiments. In particular, the large (compared with the ensemble mean) amplitude of the noise components suggests that the model response to the SST may be too weak. In contrast, the two winters were chosen because they are extreme years, and therefore the anomalies may represent truly rare occurrences of the internal atmospheric noise.

There is also the possibility that the NAO is impacted by other factors not considered here. In particular, the potential impact of autumn snow cover changes over Eurasia is discussed by Cohen et al. (2010), involving tropospheric–stratospheric coupling that leads to a more negative AO and hence NAO. Cattiaux et al. (2010) consider the role of the NAO in a warming climate, showing that analogs to the 2010 winter that occurred in past winters were in fact much colder over Europe than 2010. There is also the possibility that the NAO is itself a response to the enhanced storminess, which is in turn primarily forced by ENSO and the AO, which might, for example, explain the unusual projection of the ENSO response on the NAO. Ineson and Scaife (2009) present evidence for a stratospheric role in the transition to cold conditions in northern Europe and mild conditions in southern Europe in late winter during El Niño years. Our results do not preclude a snow and/or stratospheric connection, in that it could provide a mechanism for forcing (what is in our analysis) the noise component of the observed NAO. The ability of the GEOS-5 model to simulate a realistic stratospheric warming event necessary for such a mechanisms to work as envisioned—for example, by Cohen et al. (2010) or Ineson and Scaife (2009)—has not yet been evaluated.

Finally, the fact that the experiments were done with specified SSTs can produce unrealistic results, depending on the nature of the SST changes, and in particular whether they developed as a result of the atmospheric forcing the ocean. This is of particular concern for the North Atlantic basin and possibly the Indian Ocean, though in the latter case the SST changes appear to be part of a long-term warming trend. In any case, the key SST anomalies during these two winters had already set up by early winter, so that it is unlikely that this issue has a substantial impact on the response during February.

Acknowledgments. We wish to thank Martin Hoerling, Richard Seager, two anonymous reviewers, and the editor for their very constructive and helpful comments. Support for this work was provided by the NASA Modeling, Analysis, and Prediction (MAP) Program.

REFERENCES

Adler, R. F., and Coauthors, 2003: The Version-2 Global Precipitation Climatology Project (GPCP) monthly precipitation analysis (1979–present). *J. Hydrometeor.,* **4,** 1147–1167.

Bacmeister, J. T., M. J. Suarez, and F. R. Robertson, 2006: Rain reevaporation, boundary layer–convection interactions, and Pacific rainfall patterns in an AGCM. *J. Atmos. Sci.,* **63,** 3383–3403.

Cattiaux, J., R. Vautard, C. Cassou, P. Yiou, V. Masson-Delmotte, and F. Codron, 2010: Winter 2010 in Europe: A cold extreme in a warming climate. *Geophys. Res. Lett.,* **37,** L20704, doi:10.1029/2010GL044613.

Cohen, J., J. Foster, M. Barlow, K. Saito, and J. Jones, 2010: Winter 2009–2010: A case study of an extreme Arctic Oscillation event. *Geophys. Res. Lett.,* **37,** L17707, doi:10.1029/2010GL044256.

Collins, N., and Coauthors, 2005: Design and implementation of components in the Earth System Modeling Framework. *Int. J. High Perform. Comput. Appl.,* **19,** 341–350, doi:10.1177/1094342005056120.

Fan, Y., and H. van den Dool, 2008: A global monthly land surface air temperature analysis for 1948–present. *J. Geophys. Res.,* **113,** D01103, doi:10.1029/2007JD008470.

Feldstein, S. B., 2000: The timescale, power spectra, and climate noise properties of teleconnection patterns. *J. Climate,* **13,** 4430–4440.

Hoerling, M., 2010: Understanding the mid-Atlantic snowstorms during the winter of 2009-2010. Expert assessment report of the National Oceanic and Atmospheric Administration, 16 pp. [Available online at http://www.esrl.noaa.gov/psd/csi/images/NOAA_AttributionTeam_SnowstormReport.pdf.]

——, and A. Kumar, 2002: Atmospheric response patterns associated with tropical forcing. *J. Climate,* **15,** 2184–2203.

——, J. W. Hurrell, T. Hu, G. T. Bates, and A. S. Phillips, 2004: Twentieth century North Atlantic climate change. Part II: Understanding the effect of Indian Ocean warming. *Climate Dyn.,* **23,** 391–405, doi:10.1007/s00382-004-0433-x.

Ineson, S., and A. A. Scaife, 2009: The role of the stratosphere in the European climate response to El Niño. *Nat. Geosci.,* **2,** 32–36.

Koster, R. D., M. J. Suárez, A. Ducharne, M. Stieglitz, and P. Kumar, 2000: A catchment-based approach to modeling land surface processes in a general circulation model 1. Model structure. *J. Geophys. Res.,* **105,** 24 809–24 822.

Lin, S.-J., 2004: A vertically Lagrangian finite-volume dynamical core for global models. *Mon. Wea. Rev.,* **132,** 2293–2307.

Moorthi, S., and M. J. Suarez, 1992: Relaxed Arakawa–Schubert: A parameterization of moist convection for general circulation models. *Mon. Wea. Rev.,* **120,** 978–1002.

NWS, cited 2011: Mid Atlantic winters: Snow, wind, ice and cold. [Available online at http://www.erh.noaa.gov/lwx/winter/DC-Winters.htm.]

Richman, M. B., 1986: Rotation of principal components. *J. Climatol.,* **6,** 293–335.

Rienecker, M. M., and Coauthors, 2008: The GEOS-5 Data Assimilation System—Documentation of versions 5.0.1, 5.1.0, and 5.2.0. Tech. Rep. Series on Global Modeling and Data Assimilation, Vol. 27, NASA/TM-2008-104606, 102 pp.

——, and Coauthors, 2011: MERRA: NASA's Modern-Era Retrospective Analysis for Research and Applications. *J. Climate,* **24,** 3624–3648.

Schubert, S. D., Y. Chang, M. J. Suarez, and P. J. Pegion, 2008: ENSO and wintertime extreme precipitation events over the contiguous Unites States. *J. Climate,* **21,** 22–39.

Seager, R., Y. Kushnir, J. Nakamura, M. Ting, and N. Naik, 2010: Northern Hemisphere winter snow anomalies: ENSO, NAO and the winter of 2009/10. *Geophys. Res. Lett.,* **37,** L14703, doi:10.1029/2010GL043830.

Serreze, M., M. Clark, and D. L. McGinnis, 1998: Characteristics of snowfall over the eastern half of the United States and relationships with principal modes of low-frequency atmospheric variability. *J. Climate,* **11,** 234–250.

Smith, S., and J. O'Brien, 2001: Regional snowfall distributions associated with ENSO: Implications for seasonal forecasting, 2001. *Bull. Amer. Meteor. Soc.,* **82,** 1179–1191.

Straus, D. M., and J. Shukla, 2002: Does ENSO force the PNA? *J. Climate,* **15,** 2340–2358.